Journal of Science and Transport Technology
Journal homepage: https://jstt.vn/index.php/en

Nonlinear dynamic buckling analysis of the FG-GPLRC cylindrical and sinusoid panels with porous core under time-dependent axial compression

Nguyen Thi Phuong[1,2], Vu Minh Duc[1,2,3], Luu Ngoc Quang[4,*]
[1]Laboratory of Advanced Materials and Structures, Institute for Advanced Study in Technology, Ton Duc Thang University, Ho Chi Minh City, Vietnam, nguyenthiphuong@tdtu.edu.vn
[2]Faculty of Civil Engineering, Ton Duc Thang University, Ho Chi Minh City, Vietnam
[3]Institute of Transport Technology, University of Transport Technology, Hanoi, Vietnam
[4]Faculty of Civil Engineering, University of Transport Technology, Hanoi, Vietnam

Article info
Type of article:
Original research paper

DOI:
https://doi.org/10.58845/jstt.utt.2024.en.4.1.13-22

***Corresponding author:**
E-mail address:
quangln@utt.edu.vn

Received: 17/02/2024
Revised: 18/03/2024
Accepted: 20/03/2024

Abstract: The nonlinear dynamic buckling responses of functionally graded graphene platelet reinforced composite (FG-GPLRC) cylindrical and sinusoid panels with porous core are presented in this paper. The governing formulations are established by applying the nonlinear higher-order shear deformation theory (HSDT). an approximation technique is used to determine the stress function for complexly curved panels. Euler-Lagrange equations can be used to achieve the nonlinear motion equation. Numerical investigations are considered using the Runge-Kutta method for dynamic responses, and using the Budiansky-Roth criterion for critical dynamic buckling loads. Some discussions on the dynamic buckling responses of panels with porous core can be achieved from the numerical examples.

Keywords: Sinusoid panel; Cylindrical panel; Dynamic buckling; Higher-order shear deformation theory (HSDT); Nonlinear mechanics; Functionally graded graphene platelet-reinforced composite;

1. Introduction

Cylindrical panels and Rectangular plates are widely used in many structures in engineering fields. Therefore, a lot of researchers have posed different problems for these structures such as linear and nonlinear dynamic and static buckling behavior, vibration, and dynamic response behavior, …

Dynamic responses and vibration of functionally graded material (FGM) plates with variable delamination parameters were studied by Wang et al. [1] using the extended Chebyshev–Ritz method. Liew et al. [2] investigated the vibration behavior of coating-FGM-substrate cylindrical panels subjected to a temperature gradient across the thickness with general boundary conditions. The static behavior of viscoelastic FGM cylindrical panels under uniform pressure was studied by Norouzi and Alibeigloo [3] using the 3D elasticity theory, state space method, state space differential quadrature method, and Fourier expansion. The semi-analytical approaches for dynamic buckling

and vibration behavior of FGM cylindrical panels and doubly curved shallow shell panels were presented [4-6] using the Donnell shell theory, higher-order shear deformation theory (HSDT), and the Galerkin method.

Song et al. [7] investigated the buckling and postbuckling behavior of functionally graded graphene platelet-reinforced composite (FG-GPLRC) plates under biaxial compressions using the first-order shear deformation theory and two-step perturbation technique. Based on the classical plate theory and the Rayleigh–Ritz technique, the free vibrations of FG-GPLRC cantilever torsional plates were studied by Sun et al. [8] with variations in the transverse direction of pore and graphene. The vibration behavior of FG-GPLRC doubly curved shell panels was mentioned using the first-order shear deformation theory [9], and HSDT [10]. The complexly curved panels made from composites reinforced by graphene sheets and GPLs were mentioned in nonlinear buckling problems [11,12] and in nonlinear dynamic buckling and vibration behavior [13]. Bending behavior of sandwich beams with FGM porous core subjected to different load types by using the Ritz energy method [14].

For FGM structures with porous core, the plates, cylindrical panels, and cylindrical shells were investigated in nonlinear buckling and postbuckling problems using the Galerkin method [15-18]. The Ritz energy method was applied to investigate the nonlinear thermos-mechanical buckling and postbuckling of FG-GPLRC spherical caps and circular plates with porous core [19].

Due to the architecture and engineering requirements, complexly curved panels can be designed with several engineering equipments. The numerical-analytical algorithm for the nonlinear problem of dynamic buckling of sinusoid and cylindrical FG-GPLRC panels with porous core. The HSDT with von Karman nonlinearity is applied. By applying the like-Galerkin method, the stress function can be determined. The nonlinear motion equations are obtained using the Euler-Lagrange equations. By applying the Runge-Kutta method and the Budiansky-Roth criterion, critical dynamic buckling loads can be achieved. The significant influences of material, foundation, and geometrical properties on the dynamic buckling responses are investigated and validated.

2. Geometrical and Material designs of FG-GPLRC cylindrical and sinusoid panels with porous core

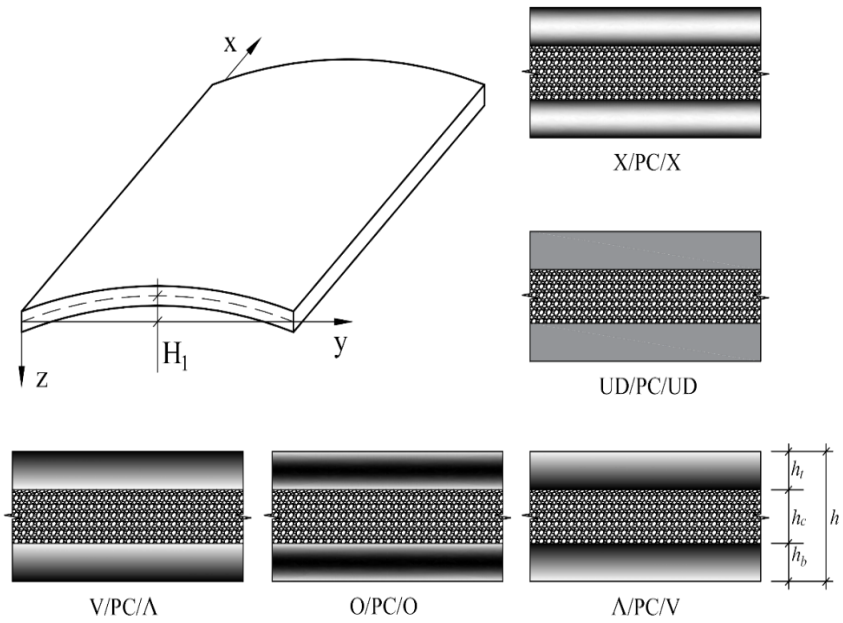

Fig. 1. Material configuration and geometry of the FG-GPLRC cylindrical and sinusoid panels with porous core

Material configuration and geometry of sinusoid and cylindrical FG-GPLRC panels and coordinate system are seen in Fig. 1, with the length of edges, rise, and thickness (a, b, h, and H_1) of curved mid-surface.

The curved y-direction surface equation of sinusoid panels is written by

$$Y_s(y) = -H_1 \sin(\pi y/b). \quad (1)$$

Based on Eq. (1), the radius equation can be obtained, as

$$R_s = \frac{\left[H_1^2\pi^2\cos^2(y\pi/b) + b^2\right]^{3/2}}{bH_1\pi^2\sin(y\pi/b)}. \quad (2)$$

The Halpin-Tsai model is used to determine the elastic modulus of panels, as

$$E_f(z) = \frac{3+3\kappa_1\tau_1\bar{V}_{GPL}(z)}{8-8\tau_1\bar{V}_{GPL}(z)}E_m + \frac{5+5\kappa_2\tau_2\bar{V}_{GPL}(z)}{8-8\tau_2\bar{V}_{GPL}(z)}E_m, \quad (3)$$

where

$$\tau_1 = \frac{-1+E_{GPL}/E_m}{\kappa_1+E_{GPL}/E_m},\ \tau_2 = \frac{-1+E_{GPL}/E_m}{\kappa_2+E_{GPL}/E_m},$$

$$\kappa_1 = 2a_{GPL}/t_{GPL},\ \kappa_2 = 2b_{GPL}/t_{GPL},$$

with E_{GPL} and E_m are respectively the elastic moduli of the GPL and matrix. The length, thickness, and width of the GPL are a_{GPL}, t_{GPL} and b_{GPL}. the GPL volume fraction $\bar{V}_{GPL}$ with $\bar{V}_M + \bar{V}_{GPL} = 1$, derived by

$$\bar{V}_{GPL}(z) = \frac{\bar{W}_{GPL}}{\bar{W}_{GPL} + (\rho_{GPL}/\rho_M)(1-\bar{W}_{GPL})}, \quad (4)$$

where ρ_{GPL} and ρ_M are respectively the mass densities of the GPLs and matrix.

In this paper, the mass distribution laws of GPL for upper and lower FG-GPLRC coatings are chosen, as [19]

+) The upper coating $\left(\frac{-h}{2} \le z \le \frac{-h_c}{2}\right)$

- UD type: $\bar{W}_{GPL} = W^*_{GPL}$; (5)

- X type: $\bar{W}_{GPL} = \left(\left|\frac{8z+4h}{h-h_c} - 2\right|\right)W^*_{GPL}$ (6)

- O type: $\bar{W}_{GPL} = \left(2 - \left|\frac{8z+4h}{h-h_c} - 2\right|\right)W^*_{GPL}$ (7)

- V type: $\bar{W}_{GPL} = \left(\frac{4z+2h_c}{h_c-h}\right)W^*_{GPL}$ (8)

- Λ type: $\bar{W}_{GPL} = \left(\frac{4z+2h}{h-h_c}\right)W^*_{GPL}$ (9)

+) The lower coating $\left(\frac{h_c}{2} \le z \le \frac{h}{2}\right)$

- UD type: $\bar{W}_{GPL} = W^*_{GPL}$; (10)

- X type: $\bar{W}_{GPL} = \left(\left|\frac{8z-4h}{h-h_c} + 2\right|\right)W^*_{GPL}$ (11)

- O type: $\bar{W}_{GPL} = \left(2 - \left|\frac{8z-4h}{h-h_c} + 2\right|\right)W^*_{GPL}$ (12)

- V type: $\bar{W}_{GPL} = \left(\frac{2h_c-4z}{h_c-h}\right)W^*_{GPL}$ (13)

- Λ type: $\bar{W}_{GPL} = \left(\frac{2h-4z}{h-h_c}\right)W^*_{GPL}$ (14)

The coefficient of thermal expansion and Poisson ratio of the panels are determined as

$$\alpha(z) = \alpha_m(1-\bar{V}_{GPL}) + \alpha_{GPL}\bar{V}_{GPL},$$
$$\nu(z) = \nu_m(1-\bar{V}_{GPL}) + \nu_{GPL}\bar{V}_{GPL}. \quad (15)$$

The porous core layer of the panels is chosen as the same material as the FG-GPLRC matrix. Effective elastic modulus and coefficient of thermal expansion can be determined as [14]

$$\begin{cases} E_c = E_m\left[1-e_0\cos(\pi z/h)\right] \\ \alpha_c = \alpha_m \\ \rho_c = \rho_m\left[1-\left(1-\sqrt{1-e_0}\right)\cos(\pi z/h)\right] \end{cases}, \quad -\frac{h_c}{2} < z < \frac{h_c}{2}, \quad (16)$$

where e_0 is the porosity coefficient ($0 \le e_0 \le 1$).

3. Physical relations and shell theory

Hooke's law for FG-GPLRC panels with porous core can be applied as

$$\begin{bmatrix}\sigma_x\\ \sigma_y\\ \sigma_{xy}\\ \sigma_{xz}\\ \sigma_{yz}\end{bmatrix}=\begin{bmatrix}Q_{11} & Q_{12} & 0 & 0 & 0\\ Q_{12} & Q_{22} & 0 & 0 & 0\\ 0 & 0 & Q_{66} & 0 & 0\\ 0 & 0 & 0 & Q_{44} & 0\\ 0 & 0 & 0 & 0 & Q_{55}\end{bmatrix}\times \times\begin{bmatrix}\varepsilon_x-\alpha\Delta T\\ \varepsilon_y-\alpha\Delta T\\ \gamma_{xy}\\ \gamma_{xz}\\ \gamma_{yz}\end{bmatrix}, \quad (17)$$

where ΔT is the temperature change, and the expressions for reduced stiffnesses Q_{ij} of the panel can be applied as

$$Q_{11}=Q_{22}=\frac{E_f(z)}{1-\left[\nu(z)\right]^2}, Q_{12}=\frac{E_f(z)\nu(z)}{1-\left[\nu(z)\right]^2},$$
$$Q_{66}=Q_{55}=Q_{44}=\frac{E_f(z)}{2\left[1+\nu(z)\right]}. \quad (18)$$

The HSDT and the von Karman nonlinearities are applied to establish the basic formulas, and the relations between strains at mid-surface with displacements and rotations are presented, as

$$\begin{Bmatrix}\varepsilon_{0x}\\ \varepsilon_{0y}\\ \gamma_{0xy}\end{Bmatrix}=\begin{Bmatrix}u_{,x}+w_{,x}^2/2+w_{,x}w_{,x}^*\\ v_{,y}+w_{,y}^2/2+w_{,y}w_{,y}^*-w/R(y)\\ v_{,x}+u_{,y}+w_{,x}w_{,y}+w_{,y}w_{,x}^*+w_{,x}w_{,y}^*\end{Bmatrix},$$
$$\begin{Bmatrix}\varepsilon_{1x}\\ \varepsilon_{1y}\\ \gamma_{1xy}\end{Bmatrix}=\begin{Bmatrix}\phi_{x,x}\\ \phi_{y,y}\\ \phi_{y,x}+\phi_{x,y}\end{Bmatrix}, \begin{Bmatrix}\varepsilon_{3x}\\ \varepsilon_{3y}\\ \gamma_{3xy}\end{Bmatrix}=-\lambda\begin{Bmatrix}w_{,xx}+\phi_{x,x}\\ w_{,yy}+\phi_{y,y}\\ \phi_{y,x}+2w_{,xy}+\phi_{x,y}\end{Bmatrix}, \quad (19)$$
$$\begin{Bmatrix}\gamma_{0xz}\\ \gamma_{0yz}\end{Bmatrix}=\begin{Bmatrix}\phi_x+w_{,x}\\ \phi_y+w_{,y}\end{Bmatrix}, \begin{Bmatrix}\gamma_{2xz}\\ \gamma_{2yz}\end{Bmatrix}=-3\lambda\begin{Bmatrix}\phi_x+w_{,x}\\ \phi_y+w_{,y}\end{Bmatrix}, \lambda=\frac{4}{3h^2}.$$

where geometrical imperfection is denoted by w^*.

The expressions of internal forces and moments are derived as follows

$$\begin{Bmatrix}N_x\\ N_y\\ N_{xy}\\ M_x\\ M_y\\ M_{xy}\\ T_x\\ T_y\\ T_{xy}\end{Bmatrix}=\begin{bmatrix}L_{11} & L_{12} & 0 & 0 & 0 & 0 & 0 & 0 & 0\\ L_{12} & L_{22} & 0 & 0 & 0 & 0 & 0 & 0 & 0\\ 0 & 0 & L_{66} & 0 & 0 & 0 & 0 & 0 & 0\\ 0 & 0 & 0 & F_{11} & F_{12} & 0 & A_{11} & A_{12} & 0\\ 0 & 0 & 0 & F_{12} & F_{22} & 0 & A_{12} & A_{22} & 0\\ 0 & 0 & 0 & 0 & 0 & F_{66} & 0 & 0 & A_{66}\\ 0 & 0 & 0 & A_{11} & A_{12} & 0 & D_{11} & D_{12} & 0\\ 0 & 0 & 0 & A_{12} & A_{22} & 0 & D_{12} & D_{22} & 0\\ 0 & 0 & 0 & 0 & 0 & A_{66} & 0 & 0 & D_{66}\end{bmatrix}\begin{bmatrix}\varepsilon_{0x}\\ \varepsilon_{0y}\\ \gamma_{0xy}\\ \varepsilon_{1x}\\ \varepsilon_{1y}\\ \gamma_{1xy}\\ \varepsilon_{3x}\\ \varepsilon_{3y}\\ \gamma_{3xy}\end{bmatrix}-\begin{bmatrix}\Phi_1\\ \Phi_1\\ 0\\ \Phi_2\\ \Phi_2\\ 0\\ \Phi_4\\ \Phi_4\\ 0\end{bmatrix}. \quad (20)$$

The shear force expressions and the higher-order shear force expressions are expressed by

$$\begin{bmatrix}Q_x\\ Q_y\\ S_x\\ S_y\end{bmatrix}=\begin{bmatrix}C_{44} & 0 & B_{44} & 0\\ 0 & C_{55} & 0 & B_{55}\\ B_{44} & 0 & E_{44} & 0\\ 0 & B_{55} & 0 & E_{55}\end{bmatrix}\begin{bmatrix}\gamma_{0xz}\\ \gamma_{0yz}\\ \gamma_{2xz}\\ \gamma_{2yz}\end{bmatrix}. \quad (21)$$

The stiffness components of panels in Eq. (20) are determined by

$$\left(L_{ij}^p, F_{ij}^p, A_{ij}^p, D_{ij}^p\right)=\int_{-h/2}^{h/2}Q_{ij}\left(1, z^2, z^4, z^6\right)dz,$$
$$(i,j=1,2,6)$$
$$\left(C_{ij}^p, B_{ij}^p, E_{ij}^p\right)=\int_{-h/2}^{h/2}Q_{ij}\left(1, z^2, z^4\right)dz, \quad (22)$$

$(i,j=4,5)$

$$(\Phi_1,\Phi_2,\Phi_4)=\Delta T\int_{-h/2}^{h/2}(\alpha Q_{11}+\alpha Q_{12})(1,z,z^3)dz,$$

The strain compatibility equation of the panels taking into account the imperfection can be established, as

$$\varepsilon_{0x,yy}-\gamma_{0xy,xy}+\varepsilon_{0y,xx}=-w_{,xx}w_{,yy}+w_{,xy}^2 -w_{,xx}^{*}w_{,yy}-w_{,xx}w_{,yy}^{*}-\frac{w_{,xx}}{R(y)}+2w_{,xy}w_{,xy}^{*}. \quad (23)$$

The stress function $\iota(x,y)$ is introduced as

$$N_y=\iota_{,xx},\quad N_x=\iota_{,yy},\quad N_{xy}=-\iota_{,xy}. \quad (24)$$

The strain compatibility equation (23) is rewritten by using Eqs. (24) and (20), as follows

$$\Xi\equiv L_{22}^{*}\iota_{,xxxx}+(L_{66}^{*}+2L_{12}^{*})\iota_{,xxyy}+L_{11}^{*}\iota_{,yyyy} +\frac{w_{,xx}}{R(y)}-w_{,xy}^2+w_{,xx}w_{,yy}+w_{,xx}w_{,yy}^{*} -2w_{,xy}w_{,xy}^{*}+w_{,xx}^{*}w_{,yy}=0, \quad (25)$$

where

$$\Pi=L_{11}L_{22}-L_{12}^2,\quad L_{11}^{*}=L_{22}/\Pi,$$
$$L_{12}^{*}=-L_{12}/\Pi,\quad L_{22}^{*}=L_{11}/\Pi,\quad L_{66}^{*}=1/L_{66},$$

4. Solutions, Boundary conditions, and Euler-Lagrange equations

The panels are considered with four simply supported and freely movable edges, as

$$\begin{aligned}&N_x=N_{0x}=-hP_x,\phi_y\big|_{x=0,a}=0,\ T_x\big|_{x=0,a}=0,\\ &N_{xy}\big|_{x=0,a}=0,\ M_x\big|_{x=0,a}=0,w\big|_{x=0,a}=0,\\ &N_y=N_{0y}=0,\quad M_y\big|_{y=0,a}=0,T_y\big|_{y=0,a}=0,\\ &N_{xy}\big|_{y=0,a}=0,\quad w\big|_{y=0,a}=0,\ \phi_x\big|_{y=0,a}=0.\end{aligned} \quad (26)$$

The deflection, rotations, and imperfect deflection of the considered panels are modeled by approximate solutions satisfying the boundary conditions (26), as

$$\begin{aligned}&w=W\sin\varphi x\sin\eta y,\\ &w^{*}=\alpha h\sin\varphi x\sin\eta y,\\ &\phi_x=\Phi_x\cos\varphi x\sin\eta y,\\ &\phi_y=\Phi_y\sin\varphi x\cos\eta y,\end{aligned} \quad (27)$$

where α is the imperfection size of the panels, the number of half waves in the x and y directions m and n, with $\varphi=m\pi/a$, $\eta=n\pi/b$

The stress function is chosen including linear and nonlinear terms, in the form [11-13]

$$\iota=\iota_1\cos2\varphi x+\iota_2\cos2\eta y+\iota_3\sin\varphi x\sin\eta y +\frac{1}{2}N_{0y}x^2+\frac{1}{2}N_{0x}y^2. \quad (28)$$

Substituting Eq. (27) and Eq. (28) into the nonlinear deformation compatibility equation (25), the like-Galerkin method is used as [11-13]

$$\begin{aligned}&\int_0^b\int_0^a\Xi\cos2\varphi x\ dxdy=0,\\ &\int_0^b\int_0^a\Xi\cos2\eta y\ dxdy=0,\\ &\int_0^b\int_0^a\Xi\sin\varphi x\sin\eta y\ dxdy=0,\end{aligned} \quad (29)$$

leads to

$$\begin{aligned}&\iota_1=V_{12}W+(W+2\alpha h)WV_{11},\\ &\iota_2=V_{22}W+(W+2\alpha h)WV_{21},\\ &\iota_3=V_{33}W,\end{aligned} \quad (30)$$

The Lagrange function is used to obtain the motion equations, as

$$\bar{U}_{Total}=\bar{U}_t-\bar{U}_{in}+\bar{U}_{ext}. \quad (31)$$

The strain energy is presented, as

$$\bar{U}_{in}=\frac{1}{2}\int_{-h/2}^{h/2}\int_0^b\int_0^a\begin{bmatrix}\sigma_{xy}\gamma_{xy}+\sigma_{xz}\gamma_{xz}\\ +\sigma_{yz}\gamma_{yz}+\sigma_x\varepsilon_x\\ +\sigma_y\varepsilon_y\\ -\alpha\Delta T(\sigma_x+\sigma_y)\end{bmatrix}dxdydz. \quad (32)$$

The work done can be determined, as

$$\bar{U}_{ext}=N_{0x}\int_0^b\int_0^a\left(\varepsilon_{0x}-\frac{1}{2}w_{,x}^2-w_{,x}w_{,x}^{*}\right)dxdy -\int_0^b\int_0^a\left\{\frac{1}{2}w\left[K_1w-K_2(w_{,xx}+w_{,yy})\right]\right\}dxdy. \quad (33)$$

with K_1 (N/m^3) and K_2 (N/m) are the stiffnesses of foundations.

Assuming that the inertia components in longitudinal and circumferential directions and the inertia components of rotations are small and can be neglected. The kinetic energy of panels can be expressed as

$$\begin{aligned}\bar{U}_t &= \frac{1}{2}\int_{-h/2}^{h/2}\int_0^b\int_0^a \rho \bar{w}_{,t}^2 dxdydz \\ &= \frac{1}{2}\int_{-h/2}^{h/2}\int_0^b\int_0^a \rho\left(w_{,t}+w_{,t}^*\right)^2 dxdydz.\end{aligned} \tag{34}$$

The Euler-Lagrange's equation is applied as

$$\begin{aligned}&\frac{d}{dt}\left(\frac{\partial \bar{U}_{Total}}{\partial \dot{W}}\right)-\frac{\partial \bar{U}_{Total}}{\partial W}=0,\\ &\frac{d}{dt}\left(\frac{\partial \bar{U}_{Total}}{\partial \dot{\Phi}_x}\right)-\frac{\partial \bar{U}_{Total}}{\partial \Phi_x}=0,\\ &\frac{d}{dt}\left(\frac{\partial \bar{U}_{Total}}{\partial \dot{\Phi}_y}\right)-\frac{\partial \bar{U}_{Total}}{\partial \Phi_y}=0,\end{aligned} \tag{35}$$

leads to

$$\begin{aligned}&\theta_{11}W+\theta_{12}\Phi_x+\theta_{13}\Phi_y+\theta_{16}W\left(W+4/3\alpha h\right)\\ &+\theta_{17}W\left(W+2\alpha h\right)\left(W+\alpha h\right)\\ &+\theta_{19}N_{0x}\left(W+\alpha h\right)-\theta_{113}+\theta_{114}\ddot{W}=0,\end{aligned} \tag{36}$$

$$\theta_{12}W+\theta_{22}\Phi_x+\theta_{23}\Phi_y=0, \tag{37}$$

$$\theta_{13}W+\theta_{23}\Phi_x+\theta_{33}\Phi_y=0, \tag{38}$$

By solving Φ_x,Φ_y from Eqs. (37) and (38), then substituting them into Eq. (36), the motion equation of the panels is obtained as

$$\begin{aligned}&\left(\theta_{12}I_{14}+\theta_{13}I_{24}+\theta_{11}\right)W+\theta_{16}W\left(W+4/3h\alpha\right)\\ &+\theta_{17}W\left(2h\alpha+W\right)\left(h\alpha+W\right)-\theta_{19}P_x h\left(h\alpha+W\right)\\ &-\theta_{113}+\theta_{114}\ddot{W}=0,\end{aligned} \tag{39}$$

where

$$I_{14}=\theta_{12}\left(\theta_{33}\theta_{12}-\theta_{13}\theta_{23}\right)\Big/\left(\theta_{23}{}^2-\theta_{33}\theta_{22}\right),$$

$$I_{24}=\left(\theta_{13}\theta_{22}-\theta_{12}\theta_{23}\right)\Big/\left(\theta_{23}{}^2-\theta_{33}\theta_{22}\right).$$

In this paper, the dynamic axial load linearly increases over time with the loading speed P_0 (GPa/s) and $P_x=P_0 t$. Eq. (39) is solved by using the fourth-order Runge-Kutta method, and the dynamic buckling loads can be determined using the Budiansky-Roth criterion [4, 5].

Neglecting the imperfect, inertial, the nonlinearities, and applying $W\to 0$ in Eq. (39), the static buckling loads are obtained, as

$$P_{xupper}=\frac{\theta_{12}I_{14}+\theta_{13}I_{24}+\theta_{11}}{h\theta_{19}}. \tag{40}$$

The critical static and dynamic buckling loads can be respectively determined to be the minimum static and dynamic buckling loads vs. the buckling modes (m,n).

5. Numerical results

Table 1. Validation of the critical static buckling loads of FGM cylindrical panels with porous core (MPa) (p=1, h =0.006m, $h_c=5h_{FG}$, $b=50h$, $a=1.5b$, $R=a/0.5$, α =0, $(m,n)=(3,1)$, ΔT =0K, K_1= 60 MN/m^3, K_2 = 0.5 MN/m).

	Source	e_0			
		0	0.2	0.5	0.8
$h_c=3h_{FG}$	Hoan et al. [18]	614.8104	589.3391	551.1321	512.9251
	Present	612.9978	586.3447	547.2530	508.3667
$h_c=5h_{FG}$	Hoan et al. [18]	597.0209	566.8193	521.5170	476.2146
	Present	595.3583	563.5668	517.0561	471.0454

Table 2. The critical dynamic buckling load (GPa) of the FG-GPLRC cylindrical and sinusoid panels with porous core (W_{GPL}^*=0.3%, h =0.02m, h_c =0.012m, $h_t=h_b$ =0.004m, e_0 =0.3, $a=b=20h$, $(m;n)$= (1;1), $H_1=1.5h$, α =0, ΔT =100K, K_1= 10 MN/m^3, K_2 = 0.1 MN/m).

Type		Static	Dynamic	
			P_0 = 1 (GPa/s)	P_0 = 2 (GPa/s)
UD/PC/UD	Sinusoid panel	2.4438	2.4800	2.4900
	Cylindrical panel	2.4080	2.4420	2.4480
X/PC/X	Sinusoid panel	2.4437	2.4810	2.4860
	Cylindrical panel	2.4079	2.4410	2.4480
O/PC/O	Sinusoid panel	2.4404	2.4740	2.4880
	Cylindrical panel	2.4047	2.4420	2.4480
V/PC/Λ	Sinusoid panel	2.4658	2.5020	2.5400
	Cylindrical panel	2.4300	2.4640	2.4700
Λ/PC/V	Sinusoid panel	2.4301	2.4630	2.4900
	Cylindrical panel	2.3944	2.4300	2.4540

In Table 1, the validation of the static buckling loads is given by the present results with the results given by Hoan et al. [18] for the FGM cylindrical panel with simply supported edges. As can be observed, a good agreement is obtained in this comparison.

By referring to the work of Wang et al. [20], the material components are chosen by graphene platelet and cooper matrix.

The critical static and dynamic buckling loads of the cylindrical and sinusoid FG-GPLRC panels are presented in Table 2. As can be observed, the static buckling loads of the panels are smaller than the corresponding dynamic buckling loads, additionally, the dynamic buckling load increases if the loading speed increases. The buckling load of the V/PC/Λ panel is greater than that of the panels with other distribution laws. The critical buckling loads of sinusoid panels are larger than those of corresponding cylindrical panels

Figure 2 investigates the dynamic buckling responses of the cylindrical and sinusoid FG-GPLRC panels with porous core. As can be observed, the maximal amplitudes of the buckling regions of the cylindrical panels are larger than those of the corresponding sinusoid panels. Figure 3 presents the effects of the graphene distribution laws on the dynamic responses of the sinusoid FG-GPLRC panels with the porous core. The slopes of the buckling region of different distribution laws do not differ significantly. Additionally, the maximal amplitude of the buckling region of the X/PC/X panel is the largest.

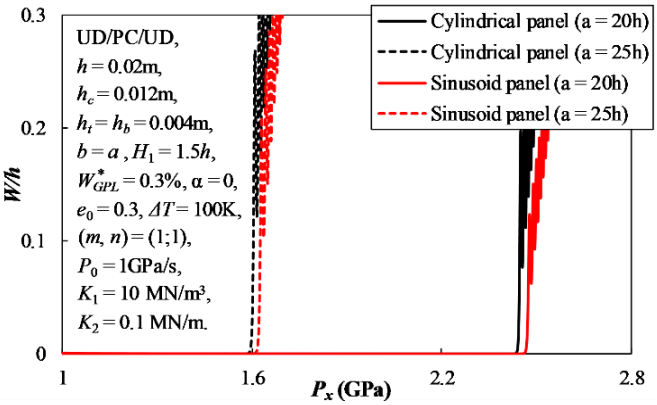

Fig. 2. Dynamic responses of sinusoid and cylindrical FG-GPLRC panels with porous core

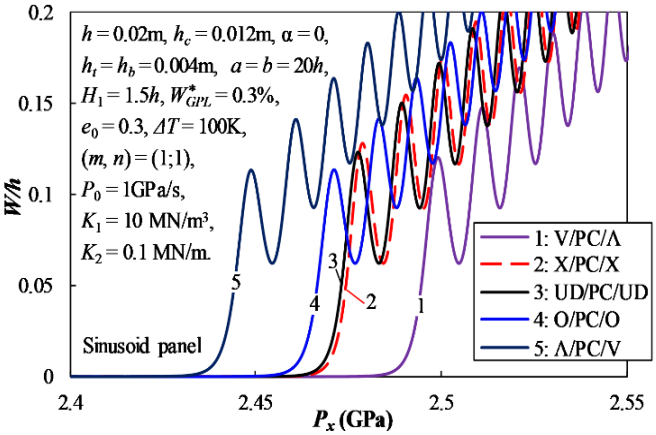

Fig. 3. Dynamic responses of sinusoid FG-GPLRC panels with different GPL distribution laws

The effects of the loading speed on the dynamic buckling responses of the cylindrical panel are investigated in Fig. 4. The critical

dynamic buckling load and the maximal amplitude of the buckling region of the panel increase as the loading speed increases. Dynamic buckling responses of sinusoid FG-GPLRC panels with different foundation parameters are shown in Fig. 5. The dynamic critical buckling loads of panels increase when the foundation stiffnesses increase. Oppositely, the slope and maximal amplitude of buckling regions do not differ significantly with different foundation stiffnesses.

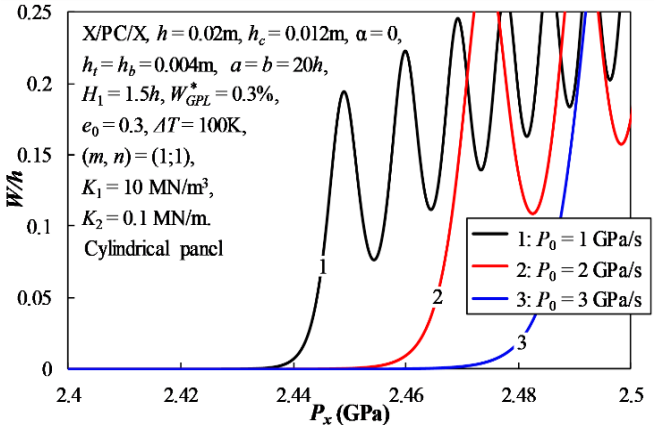

Fig. 4. Dynamic buckling responses of cylindrical FG-GPLRC panels with different loading speed

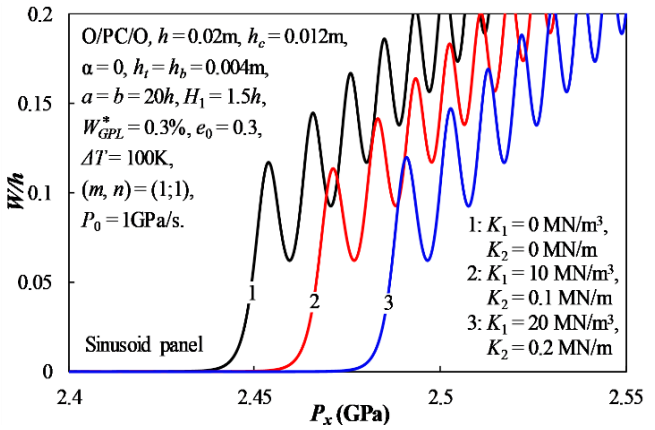

Fig. 5. Dynamic buckling responses of cylindrical FG-GPLRC panels with different foundation parameters

Effects of the porosity coefficient for porous core on the dynamic buckling responses of cylindrical FG-GPLRC panels are presented in Fig. 6. Clearly, the critical dynamic buckling loads of perfect panels decrease when the porosity coefficient for porous core increases.

For imperfect panels, the buckling region does not appear in the dynamic response curves. Figure 7 presents the dynamic buckling responses of cylindrical FG-GPLRC panels with different GPL mass fractions. The critical dynamic buckling loads of perfect panels increase when the GPL volume fraction for the porous core increases.

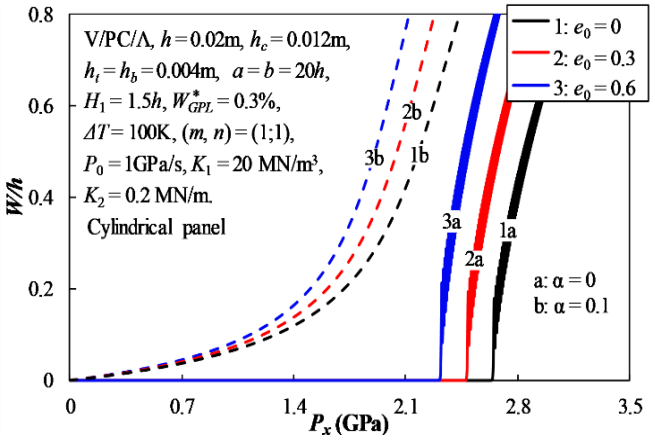

Fig. 6. Dynamic buckling responses of cylindrical FG-GPLRC panels with different porosity coefficients

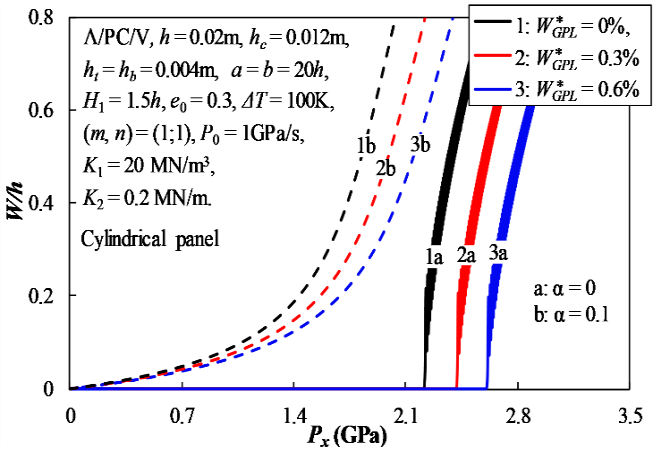

Fig. 7. Dynamic buckling responses of cylindrical FG-GPLRC panels with different GPL mass fractions

6. Conclusion

The nonlinear dynamic buckling behavior of the cylindrical and sinusoid panels made by FG-GPLRC subjected to dynamic axial compression is investigated in this paper. The investigated results give significant points as

1) The critical buckling load of the sinusoid panel is larger than that of the corresponding cylindrical panel.

2) The slopes of the buckling region of different distribution laws do not differ significantly.

The maximal amplitude of the buckling region of the X/PC/X panel is the largest.

3) The critical dynamic buckling load of the perfect panel decreases when the porosity coefficient for the porous core increases. For imperfect panels, the buckling region does not appear in the dynamic response curves.

References

[1] J.F. Wang, G. Cao, Z.W. Song, S.K. Lai. (2023). Dynamic analysis of FGM plates with variable delamination parameters by the Chebyshev–Ritz method. *International Journal of Structural Stability and Dynamics*, 23(16n18), 2340013.

[2] K.M. Liew, J. Yang, Y.F. Wu. (2006). Nonlinear vibration of a coating-FGM-substrate cylindrical panel subjected to a temperature gradient. *Computer Methods in Applied Mechanics and Engineering*, 195(9-12), 1007-1026.

[3] H. Norouzi, A. Alibeigloo. (2017). Three dimensional static analysis of viscoelastic FGM cylindrical panel using state space differential quadrature method. *European Journal of Mechanics - A/Solids*, 61, 254-266.

[4] D.H. Bich, D.V. Dung, V.H. Nam. (2012). Nonlinear dynamical analysis of eccentrically stiffened functionally graded cylindrical panels. *Composite Structures*, 94(8), 2465-2473.

[5] D.H. Bich, D.V. Dung, V.H. Nam. (2013). Nonlinear dynamic analysis of eccentrically stiffened imperfect functionally graded doubly curved thin shallow shells. *Composite Structures*, 96, 384-395.

[6] D.T. Dong, D.V. Dung. (2019). A third-order shear deformation theory for nonlinear vibration analysis of stiffened functionally graded material sandwich doubly curved shallow shells with four material models. *Journal of Sandwich Structures and Materials*, 21(4), 1316-1356.

[7] M. Song, J. Yang, S. Kitipornchai and W. Zhu. (2017). Buckling and postbuckling of biaxially compressed functionally graded multilayer graphene nanoplatelet-reinforced polymer composite plates. *International Journal of Mechanical Sciences*, 131-132, 345-355.

[8] K.C. Sun, Y.X. Hao, W. Zhang, S.W. Yang, Y.T. Cao. (2023). Effect of graphene reinforcement on free vibration and material properties of the FG-GPLRC porous cantilever torsional plate. *International Journal of Structural Stability and Dynamics*, 24(4), 2450041.

[9] H.R. Esmaeili, Y. Kiani, Y. Tadi Beni. (2022). Vibration characteristics of composite doubly curved shells reinforced with graphene platelets with arbitrary edge supports. *Acta Mechanica*, 233, 665-683.

[10] A. Wang, H. Chen, Y. Hao, Wei Zhang. (2018). Vibration and bending behavior of functionally graded nanocomposite doubly-curved shallow shells reinforced by graphene nanoplatelets. *Results in Physics*, 9, 550-559.

[11] V.H. Nam, C.V. Doan, N.T. Phuong. (2023). A new analytical approach to the nonlinear buckling and postbuckling behavior of functionally graded graphene reinforced composite laminated cylindrical, parabolic, and half-sinusoid shallow imperfect panels. *Polymer Composites*, 44(12), 8928-8945.

[12] N.T. Phuong, C.V. Doan, V.H. Nam. (2023). Postbuckling analysis of externally pressured parabola, sinusoidal and cylindrical FG-GRCL panels using HSDT. *Journal of Science and Transport Technology*, 3(2), 34-42.

[13] N.T. Phuong, V.M. Duc, N.T. Giang, L.N. Ly, N.T.T. Xuan, V.H. Nam. (2023). Nonlinear Vibration and Dynamic Buckling of Complex Curved Functionally Graded Graphene Panels Reinforced with Inclined Stiffeners. *International Journal of Structural Stability and Dynamics*.

[14] B. Srikarun, W. Songsuwan, N. Wattanasakulpong. (2021). Linear and nonlinear static bending of sandwich beams with functionally graded porous core under different distributed loads. *Composite Structures*, 276, 114538.

[15] T.M. Tu, L.K. Hoa, D.X. Hung, L.T. Hai. (2018). Nonlinear buckling and post-buckling analysis of imperfect porous plates under mechanical

loads. *Journal of Sandwich Structures and Materials*, 22(6), 1910-1930.

[16] D.Q. Chan, P.V. Hoan, N.T. Trung, L.K. Hoa, D.T. Huan. (2021). Nonlinear buckling and post-buckling of imperfect FG porous sandwich cylindrical panels subjected to axial loading under various boundary conditions. Nonlinear buckling and post-buckling of imperfect FG porous sandwich cylindrical panels subjected to axial loading under various boundary conditions. *Acta Mechanica*, 232(1), 1163-1179.

[17] V.H. Nam, N.T. Trung, L.K. Hoa. (2019). Buckling and postbuckling of porous cylindrical shells with functionally graded composite coating under torsion in thermal environment. *Thin-Walled Structures*, 144, 106253.

[18] P.V. Hoan, D.N. Mai, K.V. Phu, L.K. Hoa. (2022). Nonlinear buckling and post-buckling of imperfect FG porous sandwich cylindrical panels subjected to axial loading on elastic foundation. *Vietnam Journal of Mechanics*, 44(4), 514-525.

[19] L.N. Ly, B.T. Tu, D.T.N. Thu, D.T. Dong, V.M. Duc, N.T. Phuong. (2023). Nonlinear thermo-mechanical buckling and postbuckling of sandwich FG-GPLRC spherical caps and circular plates with porous core by using higher-order shear deformation theory. *Journal of Thermoplastic Composite Materials*, 36(10), 4083-4105.

[20] Y. Wang, R. Zeng, M. Safarpour. (2022). Vibration analysis of FG-GPLRC annular plate in a thermal environment. *Mechanics Based Design of Structures and Machines*, 50(1), 352-370.